Comparing reconstruction methods for USCT data challenge 2017

Naiara Korta Martiartu, Christian Boehm, Vaclav Hapla and Andreas Fichtner
Seismology and Wave Physics Group, Institute of Geophysics, ETH Zurich, Switzerland

CSCS Centro Svizzero di Calcolo Scientifico Swiss National Supercomputing Centre

ABSTRACT

Ultrasound Computer Tomography (USCT) is a promising candidate for breast cancer screening. It provides quantitative images of the acoustic properties of the tissue, such as speed-of-sound, attenuation and reflectivity. This information is particularly useful to differentiate tumors from benign lesions.

Conventional ray-based approaches are widely used for the reconstructions. Based on the infinite frequency approximation, they provide computationally efficient implementations, but the resulting images are limited in spatial resolution. With the need to improve the diagnostic accuracy, the applicability of imaging methods that incorporate finite frequency considerations is currently being investigated.

In this study, we compare reconstructions obtained with different imaging methods using real data provided by USCT data challenge 2017. In particular, we compare (1) time-of-flight inversion using straight rays and (2) using finite-frequency sensitivity kernels for speed-of-sound; and (3) B-mode and (4) Reverse Time Migration (RTM) for reflectivity.

DATA

We use the following datasets from USCT data challenge 2017:

- **CSIC/UCM MUBI dataset (Camacho et al. 2012):**
  - 2D acquisition system (MUBI)
  - Dominant frequency: 3.5 MHz
  - Measurements:
    - 16 emitters x 16x11 receivers x 23 rotations
  - Synthetic phantom: homogeneous background with 2 inclusions + 2 needles
    - Diameter: 9.4 cm
    - Inclusion 1: Water (2 cm diameter)
    - Inclusion 2: Gelatin (2 cm diameter)
    - Steel needles: 0.25 mm diameter

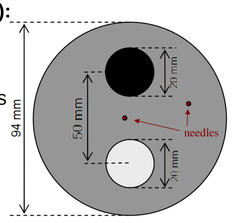

- **KIT dataset (Ruiter et al. 2017):**
  - 3D acquisition system
  - Dominant frequency: 2.5 MHz
  - Measurements:
    - 20 rotations x 157x4 emitters x 157x9 receivers
  - Turkey phantom: two olives wrapped in a turkey steak
    - Diameter: 9 cm
    - Turkey > 1550 m/s; olives 1450 m/s

IMAGING METHODS

In this section, we present (1) the forward problem of the tomographic methods used for the speed-of-sound reconstruction; and (2) the imaging conditions for reflectivity reconstruction techniques.

Speed-of-sound reconstruction

[A] Time-of-flight inversion using straight rays:

The Time-Of-Flight (TOF) t_i of the i-th ray that travels from the emitter at $\mathbf{x}_s$ to the receiver at $\mathbf{x}_r$ is computed as

$$t_i = \int_{\text{ray}} \frac{dl}{c(\mathbf{x})} \approx \sum_{j=1}^{N} \frac{l_{ij}}{c_j} \qquad (1)$$

where $c(\mathbf{x})$ is the speed-of-sound at position $\mathbf{x}$ and dl is differential arclength along the ray-path. In the discrete form, N is the number model parameters in the Region of Interest (ROI), l_{ij} is the length of the i-th ray at j-th cell and c_j is the speed-of-sound at j-th cell. By assuming straight rays, the forward problem becomes linear with respect to the slowness, i.e., the reciprocal of the speed-of-sound.

Note that the same algorithm can be used to reconstruct the attenuation information of the tissue (Li et al. 2008).

[B] Time-of-flight inversion using finite-frequency sensitivity kernels:

If finite-frequency effects are taken into account, anomalies in the TOF of the i-th ray can be related to speed-of-sound perturbations through the sensitivity kernel $K(\mathbf{x}; \mathbf{x}_r, \mathbf{x}_s)$ as

$$\delta t_i = \int_V K(\mathbf{x}; \mathbf{x_r}, \mathbf{x_s}) \delta c(\mathbf{x}) d^3\mathbf{x} \qquad (2)$$

with

$$K(\mathbf{x}; \mathbf{x_r}, \mathbf{x_s}) = \frac{-2}{c^3} \int_0^T \dot{p}(\mathbf{x}, t; \mathbf{x_s}) \dot{p}^\dagger(\mathbf{x}, T-t; \mathbf{x_r}) dt \qquad (3)$$

being $p(\mathbf{x}, t; \mathbf{x}_s)$ the pressure field due to a source located at $\mathbf{x}_s$ and T the end time. We have use the dot notation for the time derivative and the symbol † indicates the adjoint pressure field computed from the cross-correlation TOF misfit functional (Dahlen et al. 2010).

We linearize the equation (2) with respect to a homogeneous model that represents the water.

Reflectivity reconstruction

[C] B-mode technique using straight rays:

Assume that $I(\mathbf{x})$ represents the reflector image in our ROI. For the conventional B-mode technique, the image condition is given by

$$I(\mathbf{x}) = \sum_s \sum_r E\left(\mathbf{x}_r, t = \frac{||\mathbf{x}_s - \mathbf{x}|| + ||\mathbf{x} - \mathbf{x}_r||}{c(\mathbf{x})}; \mathbf{x}_s\right) \qquad (4)$$

where E indicates the envelope of the observed measurement $p(\mathbf{x}_r, t; \mathbf{x}_s)$, and the sum is over all emitters and receivers. Straight rays are assumed to compute the TOF.

[D] Reverse Time Migration (RTM):

The conventional RTM imaging condition is expressed as:

$$I(\mathbf{x}) = \sum_s \sum_r \int_0^T p(\mathbf{x}, t; \mathbf{x}_s) p^\dagger(\mathbf{x}, T-t; \mathbf{x}_r) dt \qquad (5)$$

where the adjoint field is computed by backpropagating the observed measurements (with first arrivals muted) from the receiver locations.

CSIC dataset: Speed-of-sound

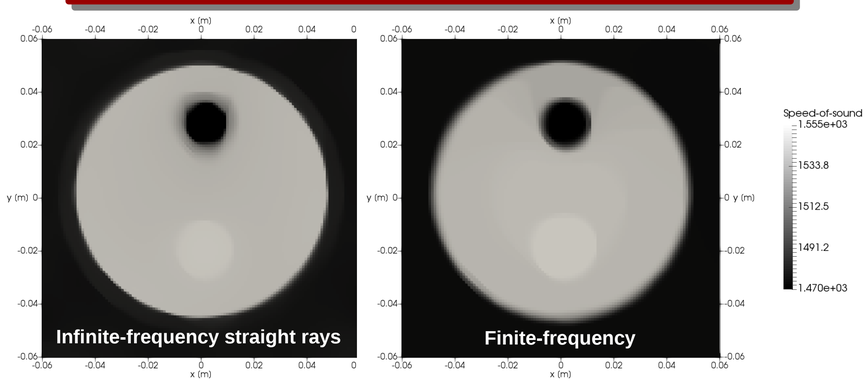

Figure 1. (From left to right) Speed-of-sound reconstructions using tomographic method [A] and [B], respectively. In both cases we have used Total Variation regularization. Note the differences in the sizes of the inclusions.

CSIC dataset: Reflectivity

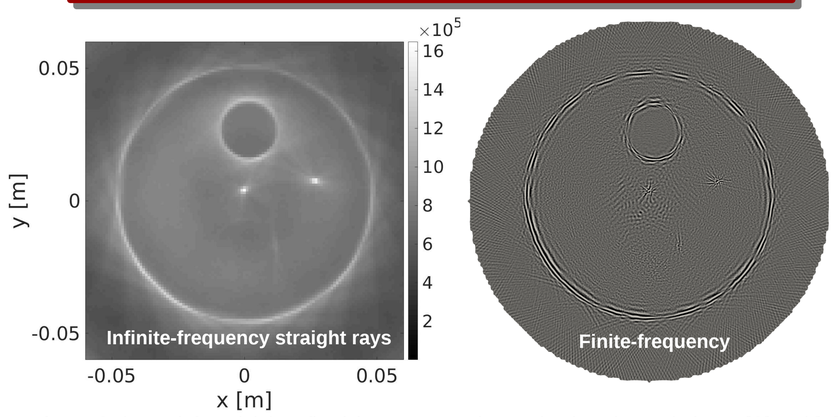

Figure 2. (From left to right) Reflectivity reconstructions using imaging techniques [C] and [D], respectively. In both cases, we have used the speed-of-sound model in Fig. 1-left to reconstruct the reflectivity images.

CSIC: B-mode + Speed-of-Sound

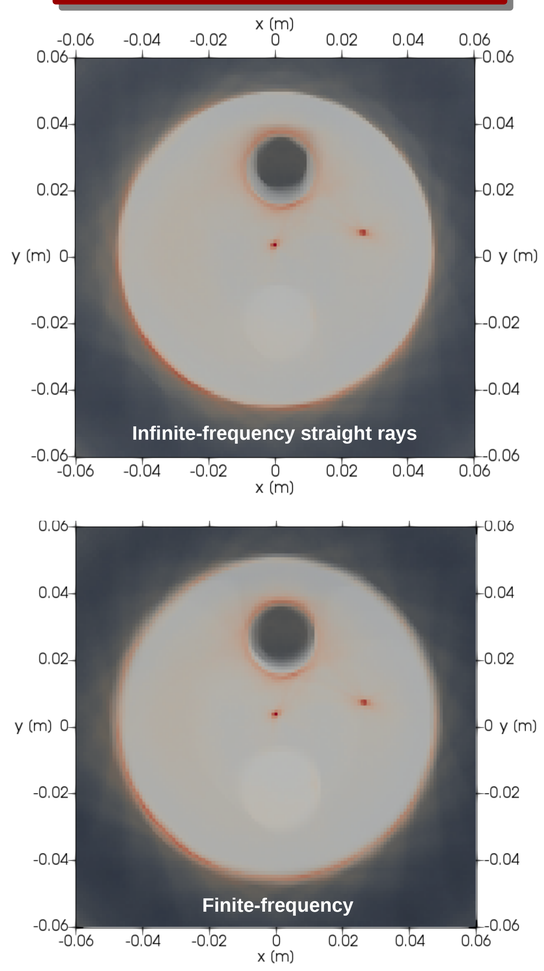

Figure 3. (From top to bottom) Superposition of B-mode image and speed-of-sound reconstructions using tomographic methods [A] and [B], respectively. The method [B] resolves the size of the inclusions more accurately.

CSIC: Attenuation

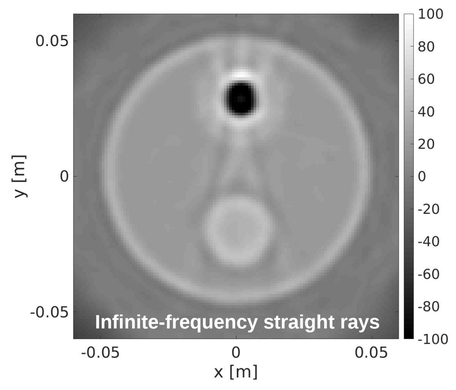

Figure 4. Attenuation reconstruction using the tomographic method [A].

KIT dataset: Speed-of-sound

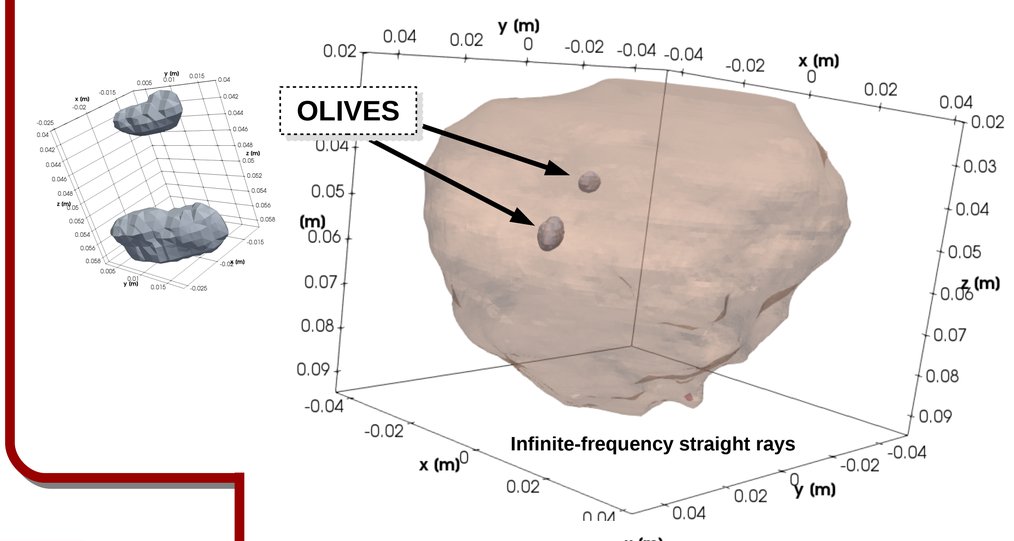

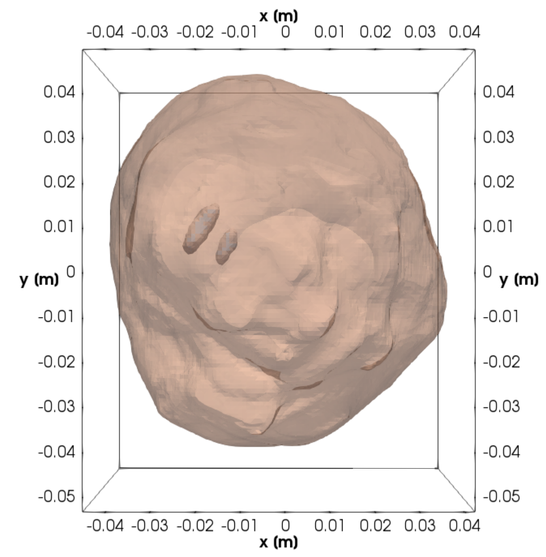

Figure 6. Side and top view of **s**peed-of-sound reconstruction using the tomographic method [A]. Total Variation regularization was applied in the inversion.

CSIC: 3D speed-of-sound reconstruction

In MUBI scanning system, the emitters and receivers are located in the same plane. When ray-based tomographic methods are used, only 2D reconstructions are possible. However, finite-frequency considerations allow us to incorporate out-of-plane effects to compute 3D sensitivity kernels, and therefore, 3D reconstructions.

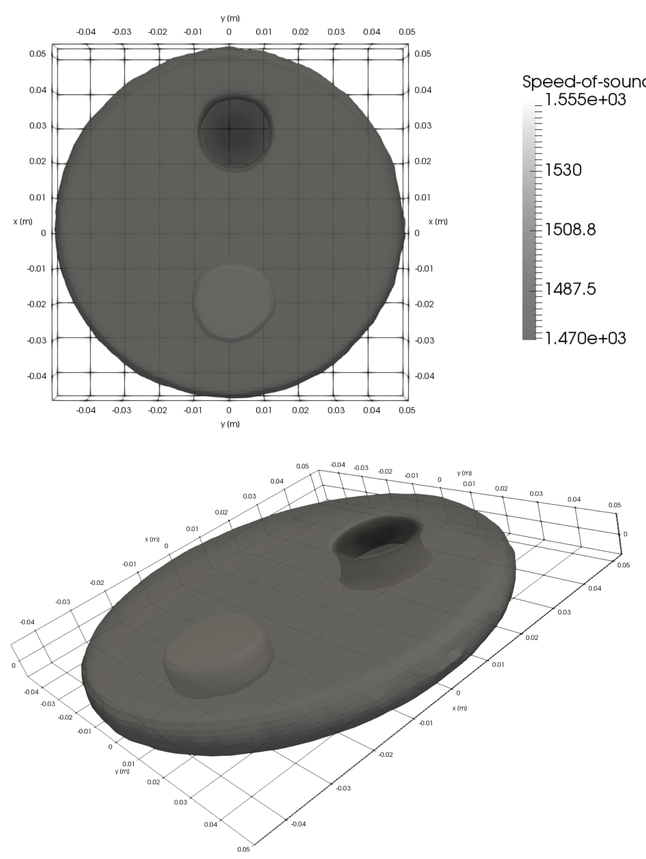

Figure 5. Top and side view of the 3D speed-of-sound reconstruction. The surrounding water was removed from the image for clarity. Total Variation regularization was applied for the inversion. Note that while the true phantom contains cylindrical inclusions, this shape is not accurately recovered due to linearization assumptions of the tomographic method.

CONCLUSIONS

Finite-frequency considerations incorporated in the method [B] provide more accurate reconstructions for the speed-of-sound. Furthermore, it allows us to compute 3D sensitivity kernels, which has the potential to enable 3D time-of-flight inversions for scanning systems based on layer-by-layer acquisition. These kernels can be computed previous to any acquisition, reducing significantly the time to the solution.

For reflectivity images, B-mode and RTM imaging techniques yield equivalent results, which validates the infinite frequency approximation of the B-mode for the studied case. Here, the data contain high frequencies. For lower frequencies, we expect RTM to perform more accurately than B-mode.

References:

J. Camacho, L. Medina, J.F. Cruza, J.M. Moreno, C. Fritsch, "Multimodal ultrasonic imaging for breast cancer detection" Archives of Acoustics, 37-3, 253-260, 2012.

N. V. Ruiter, M. Zapf, T. Hopp, H. Gemmeke, K. W. A. van Dongen, "USCT data challenge", Proc. SPIE 10139, Medical Imaging 2017: Ultrasonic Imaging and Tomography, 101391N, 2017.

C. Li, N. Duric, L. Huang, "Comparison of ultrasound attenuation tomography methods for breast imaging", Proc. SPIE 6920, Medical Imaging 2008: Ultrasonic Imaging and Signal Processing, 692015, 2008.

F. A. Dahlen, S. Hung, G. Nolet., “Fréchet kernels for finite-frequency traveltimes—I. Theory”, Geophysical Journal International, 141: 157-174, 2000.